PUBLICATIONS OF THE ASTRONOMICAL SOCIETY OF THE PACIFIC, **122**:288–298, 2010 March

NGC 2309: A Relatively Young Open Cluster Projected onto a Random Stellar Concentration

ANDRÉS E. PIATTI

Instituto de Astronomía y Física del Espacio, CC 67, Suc. 28, 1428, Ciudad de Buenos Aires, Argentina; andres@iafe.uba.ar

JUAN J. CLARIÁ

Observatorio Astronómico, Universidad Nacional de Córdoba, Laprida 854, 5000, Córdoba, Argentina; claria@oac.uncor.edu

AND

ANDREA V. AHUMADA

European Southern Observatory, Alonso de Córdova 3107, Santiago, Chile; andrea@eso.org

Received 2009 November 18; accepted 2009 December 31; published 2010 February 12

ABSTRACT. We have obtained CCD $UBVI_{KC}$ photometry down to $V \sim 22.0$ for the open cluster NGC 2309 and its surrounding field. Twenty three probable cluster members have been identified for the first time on the basis of sound photometric criteria. Because NGC 2309 is a relatively poor cluster projected onto a rich star field showing density fluctuations, the frequently used membership criteria based on stellar density profiles or proper motion measurements would not be enough to assess the star membership status if employed independently. We estimated a cluster radius of 7.9′ and a radius at half the maximum of the cluster density profile of 1.7′. Based on the best fits of isochrones computed by the Geneva group to the cluster color–magnitude and color–color diagrams, previously shifted by the cluster reddening ($E(B-V) = 0.32$) and distance ($d = 2.5$ kpc), we derived the cluster age (250 Myr) and metallicity ([Fe/H] $\simeq 0.0$). If an 8.5 kpc distance from the Sun to the center of the Galaxy is assumed, then NGC 2309 is found to be located just in front of the Perseus spiral arm.

Online material: extended table

1. INTRODUCTION

Galactic open clusters (OCs) have long been considered unrivaled objects not only to undertake structural and evolutionary studies of our own Galaxy's disk but also to enhance our understanding of stellar formation, structure, and evolution. Galactic OCs owe this privileged status to the relative ease and precision with which their reddenings, distances, and metallicities can be ascertained (see, e.g., WEBDA; Mermilliod & Paunzen 2003). As it is commonly accepted, the presence of an apparent stellar concentration in the sky is not sufficient a condition to infer that we are dealing with a genuine cluster. This criterion is probably valid in the case of globular clusters or very concentrated OCs. For most of the apparent stellar concentrations, however, it is necessary to supplement photometric data with spectroscopic and, if possible, also kinematical data (proper motions and/or radial velocities) in order to confirm their physical existence. Because the number of OCs with available spectroscopic and kinematical data is much smaller than those that have photometric data, in most cases we only count on photometric data to determine the existence of an OC. Differences in the stellar density of a certain sky region can be caused by the presence of a genuine OC or by a random fluctuation of the stellar density in that region or by the presence of interstellar material not uniformly distributed or even by some combination of these three factors. A typical example is NGC 6994 that Bassino et al. (2000) consider a 2–3 Gyr OC but that Carraro (2000) assumes to be simply a random enhancement of four bright stars above the background level rather than an OC. Because star clusters are known to evolve dynamically and stellar depletion effects eventually lead to cluster dissolution, it is probable that some unconfirmed clusters are in fact cluster remnants or fossil remains (de la Fuente Marco 1998; Bonatto et al. 2004; Gieles 2009). On the other hand, color-magnitude diagrams (CMDs) of OCs often suffer from high interstellar absorption, field star contamination, or both effects combined, which need to be corrected before deriving any cluster parameter. Sometimes, CMDs of OCs show two star sequences, one of them being the genuine cluster sequence and another that includes a chance grouping of field stars.

It is worth noticing here that more than half of the 1788 currently cataloged OCs have been poorly studied or yet unstudied. Therefore, the sole confirmation of the physical reality of cluster candidates is a valuable contribution to our knowledge of the OC system. In this context, the current article is part of a larger systematic survey aiming at obtaining good-quality photometric data not only to enlarge the sample of studied clusters but also to estimate their fundamental parameters more accurately. Thus, this study represents a further intermediate step in a more ambitious program whose goals are to obtain the fundamental parameters for some unstudied OCs or to improve the quality of observationally determined properties of some poorly studied ones.

NGC 2309 (C0653-071), also known as Cr 122 (Collinder 1931), is located ∼40° from the Galactic anticenter direction in a rich star field in Monoceros at equatorial coordinates $\alpha = 6^h56'03''$, $\delta = -7°10.5'$ (2000) and Galactic coordinates $l = 219.85°$ and $b = -2.25°$. This is a detached, moderately rich, and intermediate brightness OC of Trumpler class II2m (Ruprecht 1966). NGC 2309 has a comparatively small angular diameter of about 5′ (Lyngå 1987) quite appropriate for CCD camera analysis. The first study was performed by Nilakshi et al. (1998), who obtained CCD $UBVRI$ images in the cluster field. They derived $E(B-V) = 0.31$, $d = 2.56$ kpc, an age of ∼0.5 Gyr, and a nearly solar metal content. Moitinho (2001) also obtained CCD $UBVRI$ photometry of NGC 2309, but he did not derive the cluster parameters. This object was more recently studied by Hasegawa et al. (2008) using CCD BVI photometry. Although their results show good agreement with those of Nilakshi et al. (1998), they found NGC 2309 to be somewhat metal-poor ($[\mathrm{Fe/H}] = -0.3$).

In this study, we report the results obtained from CCD $UBVI_{KC}$ photometry down to $V \approx 22.0$ in the field of NGC 2309. The present photometric data are used to redetermine reddening, distance, age, and metallicity of NGC 2309. This article has the following layout. Section 2 presents the observational material and the data reduction. Section 3 deals with the estimation of the cluster fundamental parameters from the CMDs and color–color diagrams (ccds). Section 4 shows the analysis of the cluster structure and the estimation of the cluster dimensions. Section 5 presents a comparison of the current results with previous ones. Finally, Section 6 summarizes our findings and conclusions.

2. DATA COLLECTION AND REDUCTION

We obtained images for NGC 2309 on the night of 2000 December 25 with the $UBVI_{KC}$ filters and a 2048×2048 pixel Tektronix CCD attached to the Cerro Tololo Inter-American Observatory (CTIO, Chile) 0.9 m telescope. The detector used has a pixel size of 24 μm, yielding a scale on the chip of $0.4''$ pixel^{-1} (focal ratio $f/13.5$) and a $13.6' \times 13.6'$ field of view. We controlled the CCD through the CTIO ARCON 3.3 data acquisition system in the standard quad amplifier mode. At the beginning of the observing night, we obtained a series of bias and dome and sky flat-field exposures per filter to calibrate the CCD instrumental signature. In order to standardize our photometry, we carried out observations of standard stars of the Selected Areas PG0231 + 051, 92 and 98 of Landolt (1992). By the end of the night, we had collected a total of 46 different measures per filter for the selected standard star sample. Table 1 shows the logbook of the observations with filters, exposure times, air masses, and seeing estimates.

TABLE 1
OBSERVATIONS LOG OF NGC 2309[a]

Filter	Exposure (sec)	Air Mass	Seeing (″)
V	20	1.23	2.2
V	60	1.22	2.1
V	200	1.21	2.1
B	20	1.21	2.2
B	60	1.20	2.3
B	360	1.19	2.3
I	10	1.18	2.5
I	90	1.18	2.3
U	60	1.18	2.5
U	540	1.17	2.3

[a] Center of images: $\alpha = 06^h56^m00.0^s$, $\delta = -07°10'59.0''$ (2000.0).

We reduced the U, B, V, I_{KC} images at the Instituto de Astronomía y Física del Espacio (Argentina) with IRAF[1] using the QUADPROC package. The procedure included the bias subtraction of all the images and the flat fielding of both standard and program field images. Next, weighted combined signal-calibrator frames were employed. The resulting processed images turned out to be satisfactorily flat. We then derived the instrumental magnitudes for the standard stars from aperture photometry using DAOPHOT/IRAF routines (Stetson et al. 1990). We obtained the following transformation equations between instrumental and standard magnitudes through least-squares fits:

$$u = (3.778 \pm 0.021) + U + (0.435 \pm 0.014)X_U - (0.069 \pm 0.009)(U - B), \quad (1)$$

$$b = (2.103 \pm 0.023) + B + (0.219 \pm 0.016)X_B + (0.128 \pm 0.008)(B - V), \quad (2)$$

$$v = (1.953 \pm 0.017) + V + (0.113 \pm 0.011)X_V - (0.011 \pm 0.007)(B - V), \quad (3)$$

[1] IRAF is distributed by the National Optical Astronomy Observatories, which is operated by the Association of Universities for Research in Astronomy, Inc., under contract with the National Science Foundation.

TABLE 2
CCD $UBVI$ DATA OF STARS IN THE FIELD OF NGC 2309

ID	x (pix)	y (pix)	V (mag)	$\sigma(V)$ (mag)	n_V	$U-B$ (mag)	n_{UB}	$B-V$ (mag)	$\sigma(B-V)$ (mag)	n_{BV}	$V-I$ (mag)	$\sigma(V-I)$ (mag)	n_{VI}
1	767.192	-0.594	14.67	0.33	1	99.999	9.999	0	99.999	9.999	0	-0.388	0.386
2	1291.807	1.348	16.726	0.018	2	99.999	9.999	0	99.999	9.999	0	1.271	0.02
3	366.028	7.32	18.752	0.015	3	99.999	9.999	0	1.548	0.039	2	1.718	0.018
4	844.134	8.169	19.264	0.108	3	99.999	9.999	0	99.999	9.999	0	1.537	0.201
5	1529.707	9.534	19.532	0.053	1	99.999	9.999	0	99.999	9.999	0	1.786	0.071
6	783.278	9.71	19.889	0.018	3	99.999	9.999	0	1.709	0.39	1	1.872	0.027
7	830.509	11.464	19.379	0.016	3	99.999	9.999	0	99.999	9.999	0	1.519	0.095
8	438.79	13.43	20.809	0.078	1	99.999	9.999	0	1.67	0.207	1	1.803	0.12

NOTE.—(x, y) coordinates correspond to the reference system of Figure 1. Magnitude and color errors are the standard deviations of the mean or the observed photometric errors for stars with only one measurement.

$$v = (1.963 \pm 0.016) + V + (0.109 \pm 0.010)X_V - (0.014 \pm 0.006)(V - I), \quad (4)$$

$$i = (2.845 \pm 0.023) + I + (0.058 \pm 0.014)X_I + (0.023 \pm 0.011)(V - I), \quad (5)$$

where X represents the effective air mass, and capital and lowercase letters stand for standard and instrumental magnitudes, respectively. The coefficients were derived through the IRAF routine FITPARAM, resulting in rms errors of 0.027 for u, 0.026 for b, 0.025 for v, and 0.033 for i. Note that we performed two independent v transformations—one with $B-V$ and another with $V-I$—in order to include stars only observed in the B or I images.

The instrumental magnitudes for stars in the NGC 2309 field were obtained from point-spread function (PSF) fits using stand-alone versions of the DAOPHOT[2] and ALLSTAR[2] programs, which provided us with x- and y-coordinates and instrumental u, b, v, and i magnitudes for all stars identified in each field. For each frame, a quadratically varying PSF was derived from a selected 100 star sample, which contained the brightest, least contaminated stars. We then used the ALLSTAR program to apply the resulting PSF to the identified stellar objects and to create a subtracted image, which was used to find and measure magnitudes of additional fainter stars. The PSF magnitudes were determined using the aperture magnitudes yielded by PHOT as zero points. This procedure was repeated three times for each frame. Next, we computed aperture corrections from the comparison of PSF and aperture magnitudes using the subtracted neighbor PSF star sample.

Next, we separately combined all the measures for the shorter and longer $ubvi$ exposure sets using the stand-alone DAOMATCH[2] and DAOMASTER[2] programs. We thus obtained three tables that successively list the running number of stars; the x- and y-coordinates; the u, b, v, and i magnitudes; and the respective observational errors for each measured star. Note that stars without measured v magnitudes were excluded from the tables. The standard magnitudes and colors for all the observed stars were computed through equations (1)–(5). Once we obtained the standard magnitudes and colors, we built a master table containing the average of V, $U-B$, $B-V$, and $V-I$; their errors $\sigma(V)$, $\sigma(U-B)$, $\sigma(B-V)$, and $\sigma(V-I)$; and the number of observations for each star, respectively. Whenever there was only one measure of the magnitude and of the colors, we adopted the corresponding observational DAOPHOT error. Table 2 presents the magnitudes and colors for a total of 2275 stars measured in the field of NGC 2309. Table 2 is published in its entirety in the electronic edition of PASP. A portion is shown here for guidance regarding its form and content. Figure 1 shows the schematic finding chart of the observed cluster field, in which the sizes of the plotting symbols are proportional to the V brightness of the stars.

A simple inspection of Table 2 shows that stars with three measures of $U-B$, $B-V$, and $V-I$ colors extend from the brightest limit down to $V = 18$, 19, and 20 mag, respectively. The stars with two measures of $U-B$, $B-V$, and $V-I$ colors cover V ranges from 17.0 to 19.0 mag, from 17.5 to 20 mag, and from 18 to 21 mag, respectively. Finally, the stars with only one measure of $U-B$, $B-V$, and $V-I$ are fainter than $V = 18.0$, 19.0, and 20 mag, respectively, reaching the photometric magnitude limits. According to these crude statistics, the stars lying within the ~6 brightest magnitudes out of the ~9 mag range along which our photometry extends were measured three times. Therefore, they are the most appropriate ones to derive astrophysical information. The behavior of the photometric errors for the V magnitude and $U-B$, $B-V$, and $V-I$ colors as a function of V is shown in Figure 2, which allows us to rely on the accuracy of the morphology and position of the main cluster features in the CMDs. The resulting

[2] Program kindly provided by P. B. Stetson.

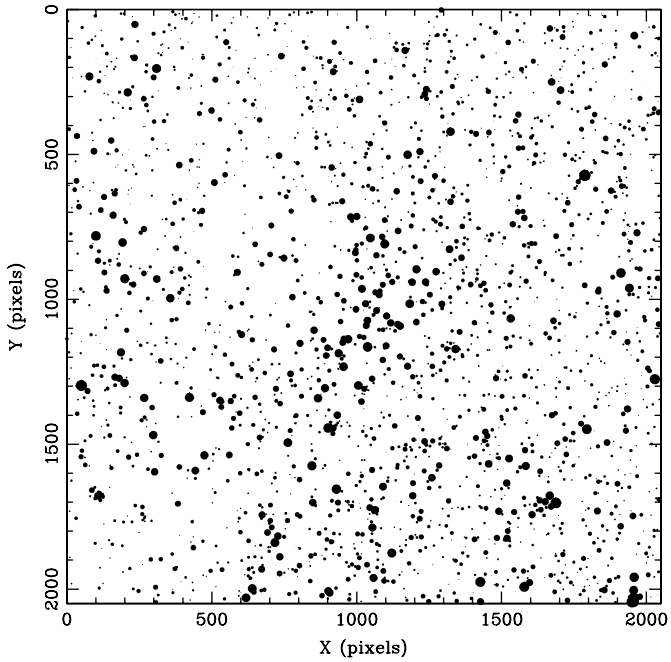

FIG. 1.—Schematic finding chart of the stars observed in the field of NGC 2309. North is up, and east is to the left. The sizes of the plotting symbols are proportional to the V brightness of the stars.

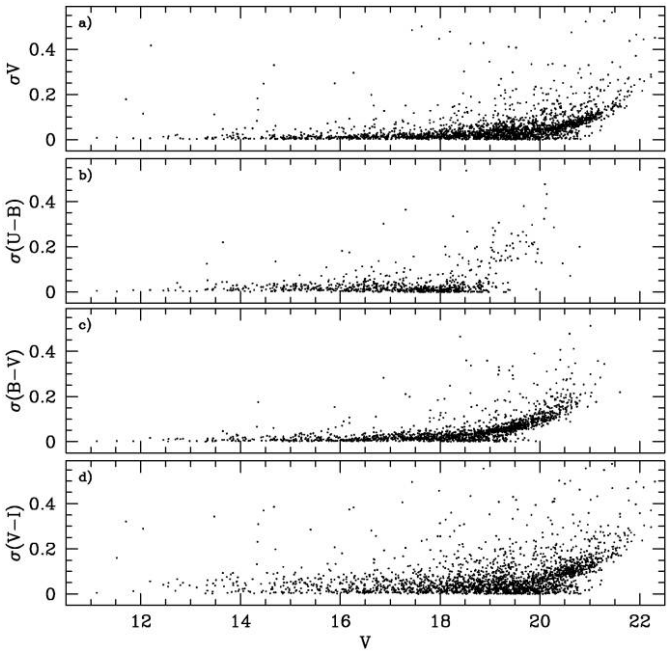

FIG. 2.—Magnitude and color photometric errors as a function of V.

CMDs and ccds are presented in Figure 3, the former showing a broad star sequence.

As far as we know, none of the previous studies by Nilakshi et al. (1998), Moitinho (2001), and Hasegawa et al. (2008) have compared their photometric data with one another's. Furthermore, we could not compare our own photometry with theirs because the published data are not available either in the WEBDA database of Mermilliod & Paunzen (2003) or upon request from the authors.

3. COLOR-MAGNITUDE AND COLOR–COLOR DIAGRAMS ANALYSIS

Without a careful analysis of the observed sequences in the CMDs, one might come to the conclusion that they are in fact the cluster's main sequences (MSs). However, all the CMDs present both cluster and field star MSs more or less superimposed. This means that we have observed both cluster and its respective foreground field affected by nearly similar reddenings, which makes it difficult to disentangle the fiducial cluster features and renders the analysis of the CMDs challenging. Fortunately, the availability of ccds involving the $U - B$ color becomes a great tool in helping us to identify possible cluster members. The criteria adopted for evaluating the membership status of the measured stars are those defined by Clariá & Lapasset (1986). Firstly, it is required that the location of a star in the three CMDs corresponds to the same evolutionary stage. The second requirement is that the location of the same star in the two ccds is close to the MS of the cluster, the maximum accepted deviation being 0.10 mag. Notice that a few probable members were discarded simply because they fall farther from the MS in some of the three CMDs, likely due to only one photometric measurement that resulted in a probably mistaken color value.

Figure 4 depicts a close up of the $(U - B, B - V)$ diagram for stars observed in the field of NGC 2309. The determination of the amount of interstellar reddening from photometry alone using techniques such as zero-age main sequence (ZAMS) fitting in a ccd requires the knowledge of the slope of the reddening line. It is well known, however, that there are variations in the reddening law throughout the Galaxy (Turner 1994), although a mean reddening slope of $E(U - B)/E(B - V) = 0.72$ is usually found for most Galactic longitudes. As can be seen in Figure 4, there is a sequence of stars with spectral types earlier than about A0 that runs nearly parallel to the unreddened color–color relation. By shifting the ZAMS given by Lejeune & Schaerer (2001), represented by the solid line, according to the $E(U - B)/E(B - V) = 0.72$ reddening line (Johnson & Morgan 1953), we find a good fit with the cluster sequence at a value of $E(B - V) = 0.32 \pm 0.02$ (dotted line). This is the lowest reddening value in the entire field, which suggests the existence of an upper cluster MS. Notice that the width of this sequence does not account for differential reddening. Therefore, we adopted this $E(B - V)$ color excess for the cluster and then looked for stars that fulfilled the requirements adopted previously. If we adopt $E(V - I)/E(B - V) = 1.25$ (Dean et al. 1978), this implies the following ratio: $E(U - B)/E(V - I) = 0.72/1.25 = 0.58$. By sliding the stars earlier than about A0

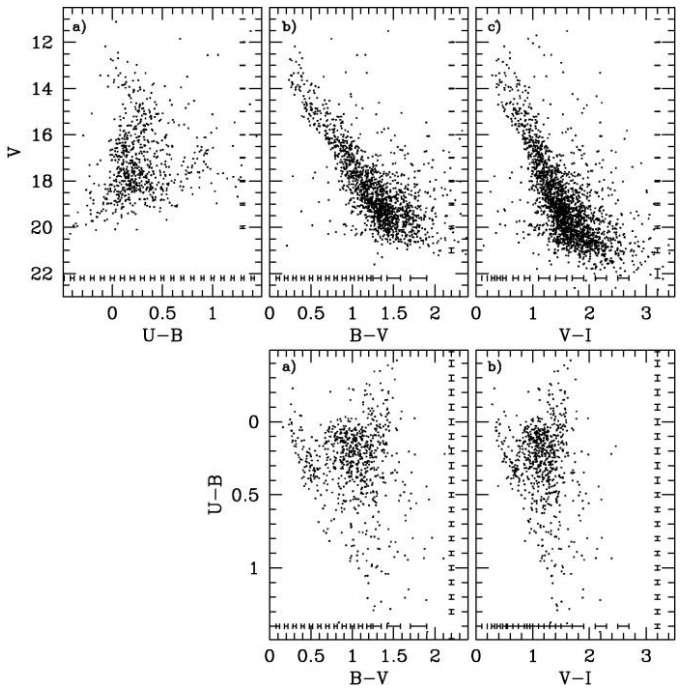

FIG. 3.—CMDs and ccds for the stars measured in the field of NGC 2309. *Top*: (a) (V, $U-B$); (b) (V, $B-V$); and (c) (V, $V-I$). *Bottom*: (a) ($U-B$, $B-V$) and (b) ($U-B$, $V-I$).

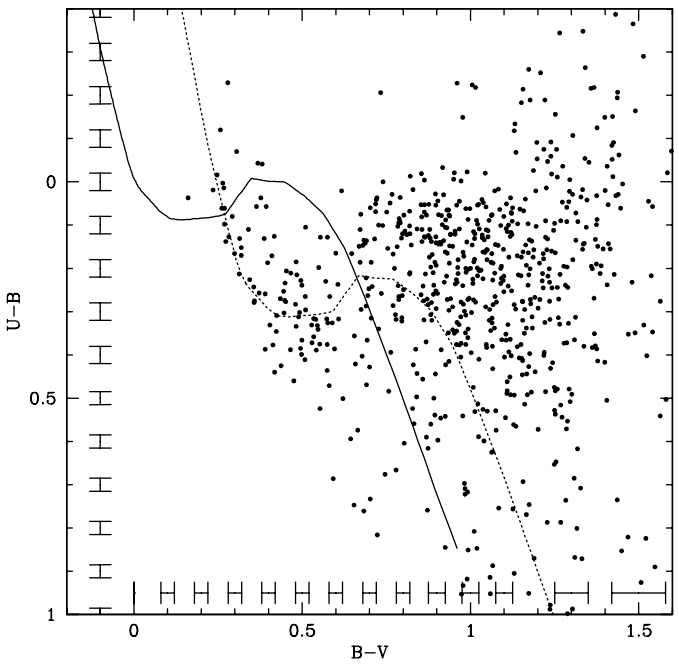

FIG. 4.—Close up of the ($U-B$, $B-V$) diagram for all the measured stars. The solid line is the unreddened ZAMS given by Lejeune & Schaerer (2001), while the dotted line represents the reddened color–color curve of the cluster.

according to this reddening line in the $U-B$ versus $V-I$ diagram, we find a good fit for $E(V-I)=0.42\pm0.03$. Furthermore, for the three CMDs we find that the ZAMSs match the same star sequences for an apparent distance modulus of $V-M_V=13.00\pm0.25$. Finally, a careful inspection of the three CMDs and of the two ccds allowed us to identify 23 photometric probable cluster members. Figure 5 shows the resulting cluster fiducial MSs in the different CMDs and ccds, wherein we have included a probable cluster giant. The solid lines represent the ZMASs of Lejeune & Schaerer (2001). Particularly, the insets in the ccds depict the intrinsic relations for luminosity class III stars taken from Schmidt-Kaler (1982) and von Braun et al. (1998).

Schlege et al. (1998; hereafter SFD) obtained full-sky maps from 100 μm dust emission. They found that in high Galactic latitude regions, the dust map correlates well with maps of H I emission. However, deviations are coherent in the sky and are especially conspicuous in regions of H I emission saturation toward denser clouds and in regions of formation of H_2 in molecular clouds (Piatti et al. 2003, 2008). Even if the SFD's reddenings would not be totally correct, they may still be valuable to compare with the reddening derived here. We used the NASA/IPAC Infrared Science Archive to extract the $E(B-V)_{\rm SFD}$ reddenings from a 2° wide image (the minimum size available) centered on the cluster. The resulting $E(B-V)_{\rm SFD}$ color excesses range from 0.88 up to 1.01 mag, with a mean value of 0.94 ± 0.04 mag. Because the $E(B-V)_{\rm SFD}$ value for NGC 2309 turned out to be approximately three times larger than both the one we estimated and the one previously published (Nilakshi et al. 1998), we assumed that such value must be saturated. It is worth considering that the range of $E(B-V)_{\rm SFD}$ values is 0.13 mag, slightly larger than 0.11, the lowest limit estimated by Burki (1975) for clusters with differential reddening. Thus we conclude that the interstellar reddening across the cluster can be considered nearly uniform within the quoted uncertainties (see also § 4 for more details).

We used the derived $E(B-V)$ color excess and apparent distance modulus $V-{\rm M}_V$ together with the most frequently used value for the $A_V/E(B-V)$ ratio (=3.2) (Straizys 1992) to obtain the cluster true distance modulus $V_o-M_V=11.98\pm0.31$ mag and the heliocentric cluster distance $d=2.50\pm0.35$ kpc. The distance error was computed with the expression

$$\sigma(d)=0.46[\sigma(V-M_V)+3.2\sigma(E(B-V))]d,$$

where $\sigma(V-M_V)$ and $\sigma(E(B-V))$ represent the estimated errors in $V-M_V$ and $E(B-V)$, respectively. By using the cluster Galactic coordinates (l, b) and the calculated heliocentric distance, we derived the cluster coordinates $(X,Y,Z)=(10.42,-1.60,-0.10)$ kpc and its Galactocentric distance $R_{GC}=10.54$ kpc, assuming the distance from the Sun to the center of the Galaxy to be 8.5 kpc.

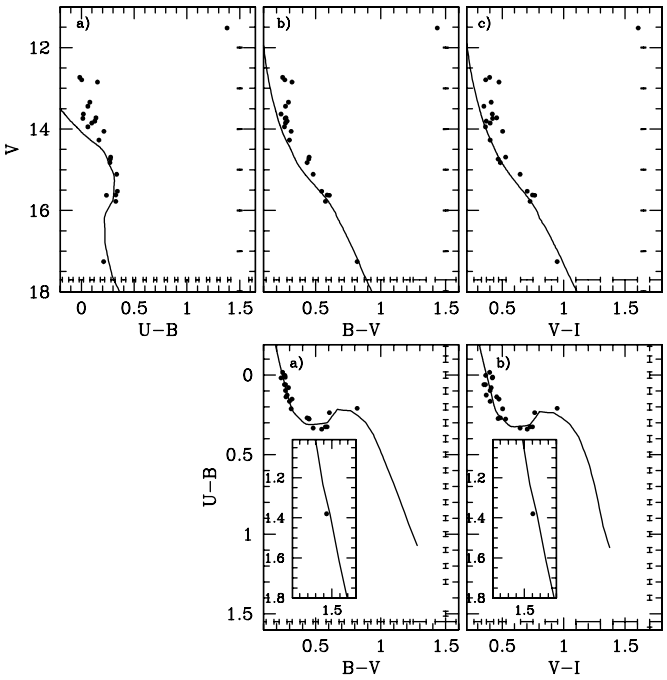

FIG. 5.—CMDs and ccds for the probable members of NGC 2309. *Top*: (a) (V, $U-B$); (b) (V, $B-V$); and (c) (V, $V-I$). *Bottom*: (a) ($U-B$, $B-V$) and (b) ($U-B$, $V-I$). The ZAMS for luminosity class V stars is plotted as a solid line. The insets in the ($U-B$, $B-V$) and ($U-B$, $V-I$) diagrams show the ZAMS for luminosity class III stars overplotted.

The widely used procedure of fitting theoretical isochrones to the observed CMDs was employed to estimate the age and the metallicity of NGC 2309. We fitted theoretical isochrones computed by Lejeune & Schaerer (2001) to the cleaned (V, $U-B$), (V, $B-V$), and (V, $V-I$) CMDs. The isochrones that cover an age range from 10^3 yr to 16–20 Gyr, in steps of $\Delta \log t = 0.05$ dex, were calculated for the entire set of nonrotating Geneva stellar evolution models. These isochrones cover star masses from 0.4–0.8 to 120–150 $M_\odot$ and star metallicities from $Z = 0.0004$ to 0.1. When selecting subsets of isochrones for different Z values to assess the metallicity effect in the cluster fundamental parameters, we preferred to choose those including overshooting effect. We followed the general rule of starting by not adopting any prearranged metallicity. Instead, we adopted chemical compositions of $Z = 0.008$, 0.020, and 0.040 for the isochrone sets that cover the metallicity range of most of the Galactic OCs studied in detail (Mermilliod & Paunzen 2003). Next, we selected a large number of isochrones and used the derived pair of distance modulus and reddening values to estimate the cluster age. The brightest magnitude in the MS, the bluest point of the turnoff, and the locus of the red giant clump were used as reference points while the fits were being made. The isochrone of $\log t = 8.40 \pm 0.10$ ($t = 250^{+65}_{-50}$ Myr) and of solar metal content turned out to be the one that most accurately reproduces the cluster features in the three CMDs, as it is shown in Figure 6.

4. CLUSTER DIMENSIONS AND STRUCTURE

The top left-hand panel of Figure 7 shows the same schematic finding chart as in Figure 1 with the photometric probable cluster members represented by filled circles. As can be seen, the cluster contains a group of stars gathered in its central region as well as some other stars sparsely distributed in a relatively larger area. The cluster stellar radial profile, represented by the solid line in the bottom right-hand panel, also accounts for such star distribution. We estimate from this diagram a cluster radius of $r = 1200$ (± 100) pixels ($7.9' \pm 0.7'$) and a radius at half the maximum of the cluster density profile of $r_c = 250$ (± 100) pixels ($1.7' \pm 0.7'$). Therefore, if we assumed the existence of a cluster corona, it would consist of an annulus of radius $r = 4.8 r_c$. The existence of coronae in OCs is a well-documented fact. Indeed, Nilakshi et al. (2002) studied the relation between core and corona in Galactic star clusters, considering the density profiles of 38 rich open star clusters built using the Digital Sky Survey. Their study shows that the coronae are most probably the outer regions around the clusters. Such a study also shows that the corona of a given cluster can exist from the very beginning of the cluster formation and that the dynamic evolution is not the reason for its occurrence. Nilakshi et al. (2002) also found that the average value of the ratio between the core radius and the annular width of the corona is 4.3 ± 1.9. Our currently determined value for NGC 2309 is in good agreement with theirs.

It is a little surprising that a large number of stars mainly concentrated to the northwest from the cluster center but not too far from it are field stars. For example, the group of stars centered at $\sim(1050, 1030)$ pixels and encompassed by a circle of $\sim$80 pixels in radius is composed of relatively bright stars, highly dispersed in the observed CMDs of Figure 3. Only from the stellar density point of view, one could expect that such

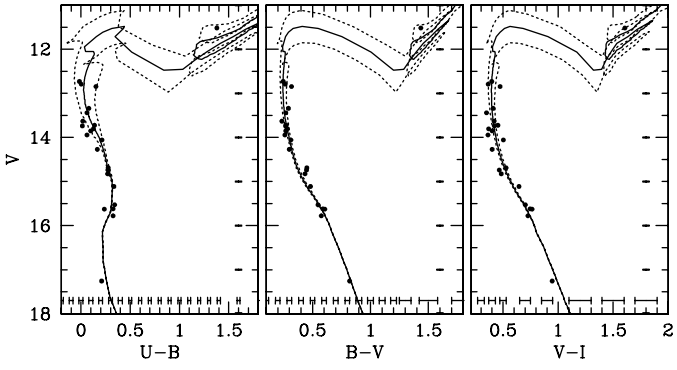

FIG. 6.—The (V, $U-B$), (V, $B-V$), and (V, $V-I$) diagrams for the probable members of NGC 2309. The adopted isochrones from Lejeune & Schaerer (2001), computed taking into account overshooting, are plotted with solid lines. For comparison purposes, we included as the dotted lines the isochrones associated to the cluster age errors.

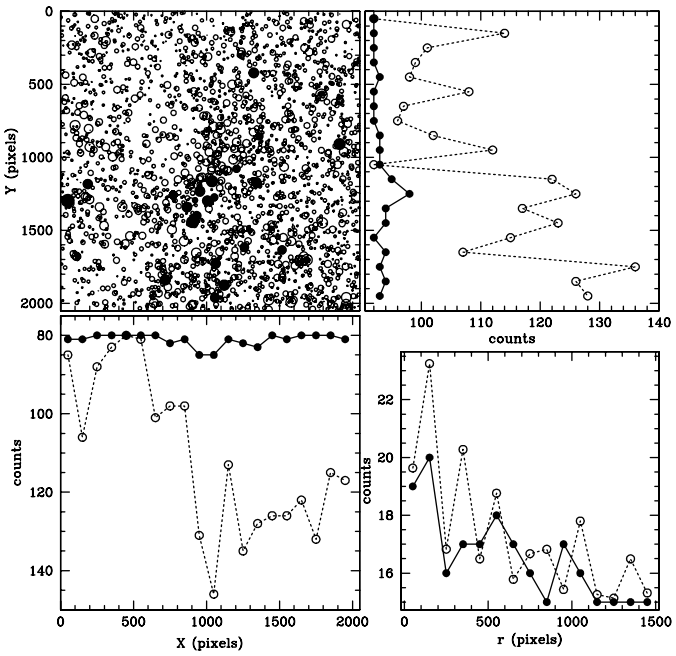

FIG. 7.—Schematic finding chart of the stars observed in the field of NGC 2309 (top left-hand panel) with its projected stellar density profiles along the x- (bottom left-hand panel) and y-directions (top right-hand panel), and its corresponding radial profile centered on the cluster (bottom right-hand panel). Open and filled circles represent field and cluster, respectively.

concentration of stars were part of the main body of NGC 2309. However, we found that this is not the case. In order to look into such phenomenon in more detail, we built stellar density profiles projected onto the x- and y-directions for all the measured stars. The stars projected along these two directions were counted within intervals of 100 pixels wide. We checked that using spatial bins from 50 to 100 pixels or from 100 to 150 pixels does not lead to significant changes in the derived profiles. We repeated this task for different I intervals from $I = 12.0$ down to 22.0 mag, in steps of $\Delta I = 1.0$ mag. Both the bottom left-hand and top right-hand panels of Figure 7 show, with dotted lines, the cumulative projected stellar density profiles along the x- and y-directions, respectively. There is an important jump in the mean stellar density roughly around $x_o = 950$ pixels and $y_o = 1100$ pixels; the region delimited by $x > x_o$ and $y > y_o$ being higher in density, on average. This implies that the stellar density of the field is not uniform and also that the cluster itself seems to be located close to the transition zone between lower and higher stellar density areas. Indeed, the cluster projected stellar density profiles along the x- and y-directions (solid lines) confirm that it is centered at $\approx(970, 1300)$ pixels. In both histograms, we have added a constant in order to set the cluster's projected profiles at the minimum background level, for comparison purposes. In addition, we find similar behaviors of the star spatial distributions when considering different I magnitude intervals. There is a more remarkable concentration of field stars near the cluster position for those with I magnitude between 14 and 15.

Because we know that variations in the stellar density can be due not only to an accidental distribution of stars along the line of sight but also to the nonuniform distribution of interstellar material, we compared our deepest I image with the 100 μm *IRAS* image covering the same area. Figure 8 depicts such a comparison, from which it is clearly visible that the northeast quadrant is affected by a slightly larger amount of dust. Although all the measured stars in the field have V and I magnitudes and considering that the stellar density distribution has a different spatial resolution than the IRSA image, a certain correspondence between both images should not be ruled out. Even though the I-band image and the IRSA images have very different resolutions, we note that the cluster may be located close to a transition region between higher and lower dust extinction.

Finally, we constructed a pseudoradial profile for the field stars centered on the cluster's center itself, with the aim to illustrate that just beside the cluster core region there exists an enhancement of field stars. To achieve that, we first performed star counts in boxes of 100 pixels a side distributed throughout the whole field of the cluster. The chosen size of the box allowed us to sample statistically the star spatial distributions, thus avoiding spurious effects mainly caused by the presence of localized groups, rows, or columns of stars. Then,

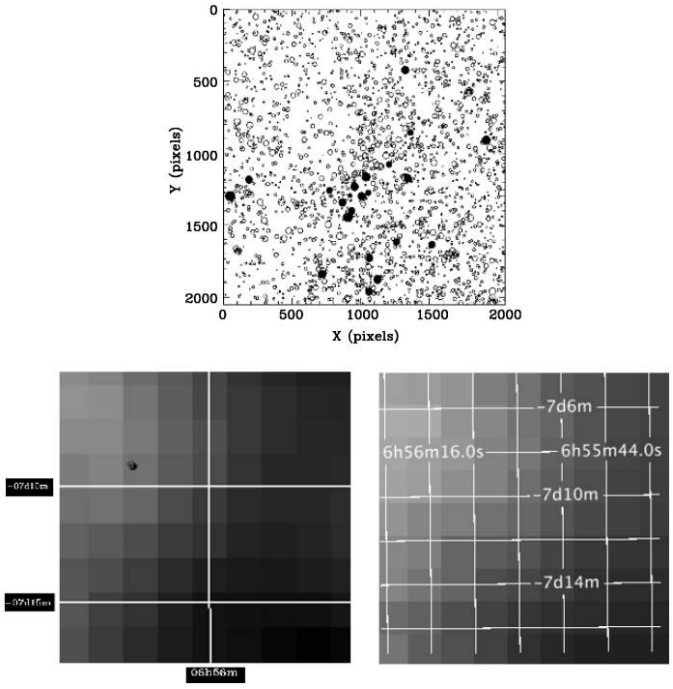

FIG. 8.—Schematic finding chart drawn in Figure 7 (top panel) compared to the 100 μm *IRAS* image (bottom left-hand panel) and IRSA dust map (bottom right-hand panel) covering the same area. Light colors mean more dust extinction.

the number of stars per unit area at a given radius r can be directly calculated through the expression

$$(n_{r+50} - n_{r-50})/[(m_{r+50} - m_{r-50})100^2], \quad (6)$$

where n_j and m_j represent the number of stars and boxes included in a circle of radius j, respectively. Note that this method does not necessarily require a complete circle of radius r within the observed field to estimate the mean stellar density at such distance. It is important to consider this fact because having a stellar density profile that extends far away from the cluster center allows us to trace the background level with more precision. The resulting density profile is represented with a dotted line in the bottom right-hand panel of Figure 7, wherein we have also added a constant to the cluster's radial profile for comparison purposes. Notice that the farther from the cluster center, the lower the field stellar density, which suggests the existence of an excess of field stars projected onto the cluster. Note that these stars do not have magnitudes or colors compatible with those of the cluster stars (see, Fig. 5). Similar results are also found by adopting, as centers for the pseudoradial profile, other positions near the cluster core region. Therefore, NGC 2309 is another example that illustrates that only a star concentration in the sky does not constitute sufficient proof of the existence of an OC.

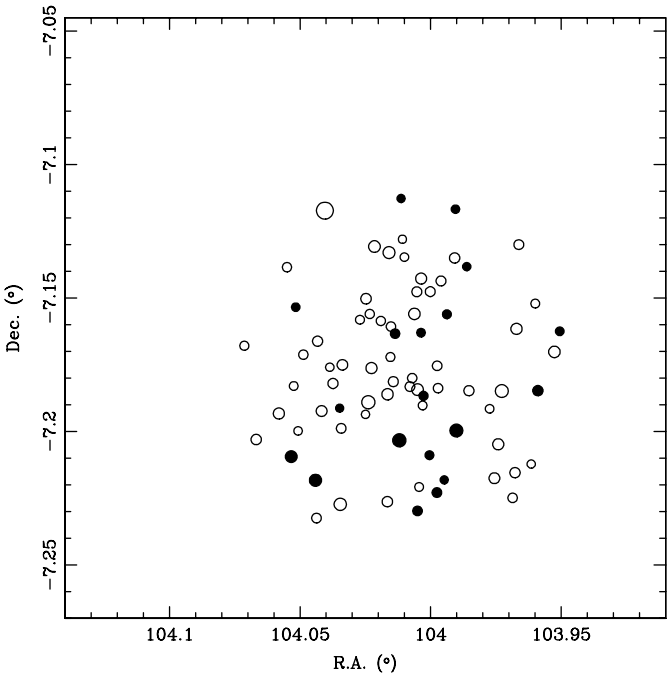

FIG. 9.—Schematic finding chart of the stars with proper motion measurements in the field of NGC 2309. Open and filled circles represent stars with membership probabilities lower and higher than 70%, respectively, according to Dias et al. (2006).

5. ANALYSIS OF PROPER MOTIONS

Based on position and proper motion measurements provided by the Second U.S. Naval Observatory CCD Astrograph Catalog (UCAC2) (Zacharias et al. 2004), Dias et al. (2006) applied a statistical method to obtain membership probabilities for 78 stars in the cluster field. On the one hand, they determined the cluster mean proper motions by discarding stars with proper motions that differ from the mean by more than three standard deviations. On the other hand, they fitted the observed distribution of proper motions with two overlapping normal bivariate frequency functions: an elliptical one for the field stars and a circular one for the clusters. Figure 9 shows a schematic finding chart for all these stars. For comparison purposes, this figure covers a similar area as in Figure 1. It presents stars with probabilities (P) of being cluster members lower and higher than 70% represented by open and filled circles, respectively. Surprisingly, the stars with higher membership probabilities do not appear clumpy but sparsely distributed through the embraced field. Moreover, most of the brighter stars seem to belong to the field.

Forty eight out of the 78 stars of Dias et al. (2006) have three measures of their V magnitudes and $U - B$, $B - V$, and $V - I$ colors in our present photometry. They are depicted in Figure 10 with the same symbols as in Figure 9 (filled circles for $P > 70\%$). We also drew the ZAMSs with solid lines once the cluster sequences were properly shifted by using the cluster color excesses $E(B - V)$ and $E(V - I)$ and the apparent distance modulus. At first glance, the stars considered to be members by Dias et al. (2006) ($P > 70\%$) do not seem to trace the cluster MS but rather they appear to belong to the star field. Moreover, a great dispersion in the CMDs and ccds is also observed among the stars with $P < 70\%$. They are also mostly field stars. Thus, if we applied the photometric criteria described in § 3 to discriminate members and nonmembers, we would find scarcely seven stars fulfilling such criteria.

The resulting mean proper motions of these seven stars are $\mu_\alpha \cos(\delta) = (-1.9 \pm 4.2)$ mas/yr and $\mu_\delta(-4.9 \pm 4.3)$ mas/yr. These mean values agree reasonably well with those derived for the cluster by Dias et al. (2006) $(0.65 \pm 0.79, -4.38 \pm 0.79)$ mas/yr. Note, however, that the errors for the proper motion measurements quoted in the UCAC2 range from 4 to 7 mas/yr for stars with V magnitudes between 12 and 16. Hence, no final result can be figured out regarding the cluster dynamics until accurate kinematical data for a larger sample of stars are obtained. For instance, it would be desirable to have proper motions available for the remaining 16 photometric probable cluster members ($V < 15$ mag), which are not included in Dias et al. (2006)'s sample. This is necessary to get a significant statistical sample of stars to compare photometric and kinematic membership probabilities. In fact, only three stars in both Dias et al. (2006) and in the current samples are found to be probable cluster members, whereas 31 stars are considered nonmembers as much by Dias et al. (2006) as by our photometric criteria. The mean proper motions of the former are $(-4.4 \pm 1.9, -1.5 \pm 1.4)$ mas/yr. By analogy to what we mentioned at the end of

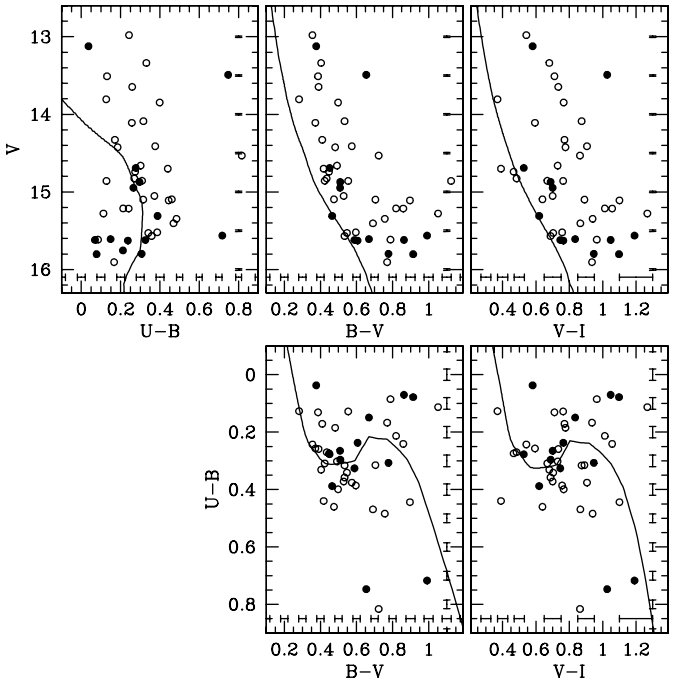

FIG. 10.—The (V, $U-B$), (V, $B-V$), and (V, $V-I$) diagrams (*top*) and ($U-B$, $B-V$) and ($U-B$, $V-I$) diagrams (*bottom*) of the stars with proper motion measurements in the field of NGC 2309. Open and filled circles represent stars with membership probabilities lower and higher than 70%, respectively, according to Dias et al. (2006).

§ 4, we conclude that NGC 2309 is an example in the sense that sometimes the proper motions do not constitute by themselves proof of the existence of a star cluster.

5.1. Comparison with Previous Results

Nilakshi et al. (1998) performed CCD $UBVRI$ observations within a field of $6^\circ \times 6^\circ$ centered on the cluster and derived $E(B-V) = 0.31 \pm 0.05$, an apparent distance modulus $V - M_V$ corresponding to a distance $d = 2.56 \pm 0.25$ kpc and a solar metal content. Their results are in very good agreement with those obtained in our present study. Although they did not present CMDs and ccds cleaned from field star contamination, they based their fundamental parameter estimates on stars brighter than $V = 17$ mag and proceeded in a similar way as we described in § 3. We think that the ($U-B$, $B-V$) diagram for those stars allowed them to figure out the cluster sequence. On the other hand, Hasegawa et al. (2008) also obtained CCD BVI photometry in the cluster field from which they derived a color excess $E(V-I) = 0.38$, a heliocentric distance of 2.65 kpc, an age of 0.6 Gyr, and a metal content of $[\mathrm{Fe/H}] = -0.3$ dex for NGC 2309. While their cluster reddening and distance values are in good agreement with those obtained by Nilakshi et al. (1998) as well as with ours, the age and metallicity they derived are different from the ones we obtained here. As far as we can tell, Hawegawa et al. simply performed circular extractions from a region close to the cluster center adopted by us. For this reason, their corresponding CMDs are highly blurred by field stars (see their fig. 2).

The position of NGC 2309 in the Galaxy, the interstellar extinction affecting it, and its age do seem to be in very good agreement with the generally accepted picture of the structure of the Galactic disk. To prove such assertion, we first searched for clusters located at $(l,b)_{\mathrm{cluster}} = (l,b)_{\mathrm{NGC2309}} \pm 5^\circ$ in order to examine the interstellar absorption law along the line of sight to NGC 2309. We decided to use the recently updated version available (February 2009) of the OC catalog by Dias et al. (2002). It provides information on the fundamental parameters for 1788 objects and includes the previous catalogs of Lyngå (1987) and of Mermilliod & Paunzen (2003). New objects and previously uncataloged data have now been included in the Dias et al. (2002) catalog (February 2009). We found 29 OCs in the aforementioned direction out of which 14 have already known heliocentric distances, $E(B-V)$ color excesses, and ages. The result of our search shows that further work is required to increase the number of Galactic OCs studied in detail.

The reddening and distance derived here for NGC 2309 place this object among the relatively most reddened and distant known OCs projected toward the direction considered, a result that is illustrated in Figure 11. The upper left-hand panel of this figure shows the distribution of the selected clusters (open circles) and NGC 2309 (filled circle) in the Galactic (X,Y) plane. The Sun is assumed to be located at $(X,Y) = (8.5, 0)$. We drew with a solid line the Perseus spiral arm traced by Drimmel & Spergel (2001). Note that the distance between the outermost and the innermost selected clusters is ~4.3 kpc. The upper right-hand panel in Figure 11 shows the relationship between the visual interstellar absorption A_V and the distance d from the Sun. For the sake of comparison, we also included the relationship between A_V and d corresponding to the Baade's window ($(l,b) = (1^\circ, -3.9^\circ)$) obtained by Ng et al. (1996), which is represented by a solid line. It can be seen in both panels that the presence of the Perseus spiral arm—schematically drawn in the figure—causes a large dispersion in the interstellar absorption A_V values in the direction considered. Indeed, the visual absorption affecting clusters located in front of the Perseus spiral arm is found to follow approximately the Baade's window law, while those placed behind it (NGC 2286 and Dias 3) are affected by a visual absorption larger by more than half a magnitude than the value expected from the Baade's window law. NGC 2286 is ~2 kpc closer to the Sun than Dias 3 and still has a similar visual absorption mainly produced by the Perseus spiral arm. Ruprecht 4, which is practically at the same distance as Dias 3 but more than 0.4 kpc below the Galactic plane (see bottom left-hand panel of Fig. 11), is about one magnitude less absorbed than Dias 3, due to the fact that the line of sight to it does not cross the Perseus spiral arm. Finally, we find some hints indicating a trend in the sense that the outermost a cluster in the Galactic

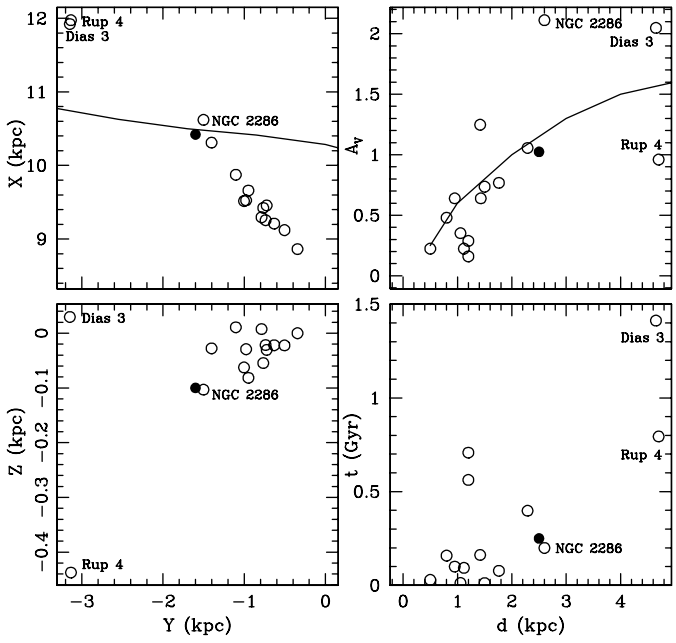

FIG. 11.—The relationship between the Galactic coordinates X and Y (*upper left*), between the distance d from the Sun and the visual interstellar absorption A_V (*upper right*), between the Galactic coordinates Y and Z (*bottom left*), and between the distance d from the Sun and age (*bottom right*) for known OC projected in the line of sight to NGC 2309. Selected clusters and NGC 2309 are represented by open circles and by a filled circle, respectively. The Perseus spiral arm is shown in the upper left-hand panel. The relationship between d and A_V for the Baade's window is indicated in the upper right-hand panel.

disk, the older it is, as previously claimed by Tadross et al. (2002); Bonatto et al. (2006), among others.

6. SUMMARY

New CCD $UBVI_{KC}$ photometry in the field of the OC NGC 2309 is reported here. The analysis of the photometric data leads to the following main conclusions:

1. NGC 2309 is a relatively poor OC projected onto a rich star field in Monoceros that shows stellar density fluctuations. Indeed, an important concentration of bright stars appears to be projected near the cluster core region.

2. We identified for the first time 23 probable cluster members on the basis of sound photometric criteria. These stars are found to be affected by color excesses of $E(B-V) = 0.32 \pm 0.02$ and $E(V-I) = 0.42 \pm 0.03$. They are located at a heliocentric distance of $d = 2.50$ kpc, just in front of the Perseus spiral arm, if a 8.5 kpc distance from the Sun to the center of the Galaxy is assumed.

3. Once the cluster center was determined, the cluster radial density profile was constructed. We estimated a cluster radius of $7.9'$ and a radius at half the maximum of the cluster density profile of $1.7'$.

4. Estimates of the cluster age and metallicity were obtained from the comparison of the cluster $(V, U-B)$, $(V, B-V)$, and $(V, V-I)$ CMDs with theoretical isochrones of the Geneva group. Our analysis yielded an age of $t = 250$ Myr and a metal abundance similar to that of the Sun.

5. From the analysis of the proper motions provided by the UCAC2 for the stars of the cluster region, we can conclude that NGC 2309 is an example that shows that sometimes the proper motions do not constitute proof of the existence of a star cluster by themselves.

We are gratefully indebted to the CTIO staff for their hospitality and support during the observing run. We thank the reviewer whose comments and suggestions have helped us to improve the manuscript. This work was partially supported by the Argentinian institutions CONICET, SECYT (Universidad Nacional de Córdoba), and Agencia Nacional de Promoción Científica y Tecnológica (ANPCyT). This work is based on observations made at Cerro Tololo Inter-American Observatory (Chile), which is operated by AURA, Inc., under cooperative agreement with the National Science Foundation.

REFERENCES

Bassino, L. P., Waldhausen, S., & Martínez, R. E. 2000, A&A, 355, 138
Bonatto, C., Bica, E., & Pavani, D. B. 2004, A&A, 427, 485
Bonatto, C., Kerber, L. O., Bica, E., & Santiago, B. X. 2006, A&A, 446, 121
Burki, G. 1975, A&A, 43, 37
Carraro, G. 2000, A&A, 357, 145
Clariá, J. J., & Lapasset, E. 1986, AJ, 91, 326
Collinder, P. 1931, Ann. Obs. Lund, 2, 1
Dean, F. J., Warren, P. R., & Cousins, A. W. J. 1978, MNRAS, 183, 569
de la Fuente Marco, R. 1998, A&A, 333, L 27
Dias, W. S., Alessi, B. S., Moitinho, A., & Lepine, J. R. D. 2002, A&AS, 141, 371
Dias, W. S., Assafin, M., Flório, V., Alessi, B. S., & Líbero, V. 2006, A&A, 446, 949
Drimmel, R., & Spergel, D. N. 2001, ApJ, 556, 181
Gieles, M. 2009, Proc. IAU Symp. No. 266, eds. de Grijs, R., & Lépine, J. R. D., astro_ph/0909.4317v2
Johnson, H. L., & Morgan, W. W. 1953, ApJ, 117, 313
Hasegawa, T., Sakamoto, T., & Malasan, H. L. 2008, PASJ, 60, 1267
Landolt, A. 1992, AJ, 104, 340
Lejeune, T., & Schaerer, D. 2001, A&A, 366, 538
Lyngå, G. 1987, Catalogue of Open Cluster Data (Strasbourg: Centre de Données Stellaires)
Mermilliod, J.-C., & Paunzen, E. 2003, A&A, 410, 511
Moitinho, A. 2001, A&A, 370, 436
Ng, Y. K., Bertelli, G., Chiosi, C., & Bressan, A. 1996, A&A, 310, 771
Nilakshi, Pandey, A. K., & Mohan, V. 1998, Bull. Astron. Soc. India, 26, 555
Nilakshi, Sagar, R., Pandey, A. K., & Mohan, V. 2002, A&A, 383, 153

Ruprecht, J. 1966, Bull. Astron. Inst. Czechoslovakia, 17, 33
Piatti, A. E., Geisler, D., Bica, E., & Clariá, J. J. 2003, MNRAS, 343, 851
Piatti, A. E., Geisler, D., Sarajedini, A., Gallart, C., & Wischnjewsky, M. 2008, MNRAS, 389, 429
Schlegel, D. J., Finkbeiner, D. P., & Davis, M. 1998, ApJ, 500, 525 (SFD)
Schmidt-Kaler, Th. 1982, Landolt-Bornstein, Numerical Data and Functional Relationships in Science and Technology, New Series, group VI, Vol. 2b, eds. Schaifers, K., & Voigt, H. H. (Berlin: Springer Verlag)
Stetson, P. B., Davis, L. E., & Crabtree, D. R. 1990, in ASP Conf. Ser. 8, CCDs in Astronomy (San Francisco: ASP), 289
Straizys, V. 1992, Multicolor Stellar Photometry (Tucson, Arizona: Pachart Publishing House)
Tadross, A. L., Werner, P., Osman, A., & Marie, M. 2002, NewA, 7, 553
Turner, D. G. 1994, RMxAA, 29, 163
von Braun, K., Chiboucas, K., Kelly Minske, J., & Salgado, J. F. 1998, PASP, 110, 810
Zacharias, N., Urban, S. E., Zacharias, M. I., Wycoff, G. L., Hall, D. M., Monet, D. G., &Rafferty, T. J.2004, AJ, 127, 3043